Eur. Phys. J. B **24**, 291–295 (2001)
DOI:

THE EUROPEAN PHYSICAL JOURNAL B
EDP Sciences

Damage processes in Fe_3O_4 magnetic insulator irradiated by swift heavy ions. Experimental results and modelisation

A. Fnidiki[1,a], F. Studer[2], J. Teillet[1], J. Juraszek[1], H. Pascard[3], and S. Meillon[3]

[1] GPM[b], CNRS-Université de Rouen, 76821 Mont-Saint-Aignan Cedex, France
[2] CRISMAT[c], ISMRA, 14050 Caen Cedex, France
[3] Laboratoire des Solides Irradiés, École Polytechnique, Route de Saclay, 91128 Palaiseau, France

Received 18 April 2001 and Received in final form 24 July 2001

Abstract. The behavior of the magnetic properties of magnetite Fe_3O_4 irradiated by swift heavy ions is investigated by magnetization measurements. Although there is no induced structural phase transformation, both coercive field and saturation magnetization are sensitive to ion irradiation and exhibit different behaviors depending on the ion fluence range. In the low fluence regime, the coercive field increases, which is evidence for a strong pinning of magnetic domain boundaries by the induced defects. The magnetization shows a decrease in the saturation value and tends to reorient perpendicularly to the ion track axis. At high fluence, the initial magnetic properties of the sample are nearly restored. The changes in the magnitude and the direction of magnetization are interpreted by magnetostrictive effects related to the stress induced by irradiation. A phenomenological model is applied to reproduce the fluence evolution of the saturation magnetization, assuming relaxation of the stress induced around the core of defects of the tracks by overlapping effects at high fluence. The results are compared to those obtained in the case of yttrium iron garnet $Y_3Fe_5O_{12}$.

PACS. 61.80.Jh Ion radiation effects – 75.60.-d Domain effects, magnetization curves, and hysteresis – 85.70.Ge Ferrite and garnet devices

1 Introduction

The damage induced in magnetic insulators by swift heavy ion irradiation consists of latent tracks, generally in the form of cylindrical volumes of amorphous material extending along the ion path. In the yttrium iron garnet ($Y_3Fe_5O_{12}$ or YIG), the amorphous nature of these latent tracks has been confirmed by high resolution transmission electron microscopy (HRTEM) and Mössbauer spectrometry [1–4]. In addition, the latter technique showed that in YIG, heavy-ion irradiation effects are able to rotate the magnetization parallel to the ion beam direction, *i.e.*, to the latent track axis [5]. This rotation was interpreted on the basis of magnetostrictive effects induced by the pressure generated in the crystalline ferromagnetic material surrounding the amorphous paramagnetic latent tracks [6]. The volume fractions of these two phases and of the resulting undamaged regions were studied as a function of the fluence by Fnidiki *et al.* [7].

In contrast, observation by HRTEM of defects induced by GeV-Pb ion irradiation in magnetite Fe_3O_4 did not reveal the presence of any amorphous phase [4]. Discontinuous latent tracks of spherical defects, surrounded by a stressed shell, were observed at low fluences. At high fluences, the stressed shell, that surrounds the ion track, was found to disappear, indicating relaxation effects. Moreover, the room temperature Mössbauer spectrometry confirmed the crystalline nature of the damaged regions and gave evidence for an induced reorientation of the magnetic hyperfine field perpendicularly to the tracks axis.

In this article, we present magnetic measurements in magnetite irradiated by swift heavy ions. A phenomenological model, which was previously applied to YIG but was not described in detail, will be presented and applied to magnetite in order to explain and reproduce quantitatively the dependence of the magnetization on the ion fluence.

2 Experiments

As previously published [8], the magnetite samples were synthezised using a classical ceramic method. Cores of

[a] e-mail: abdeslem.fnidiki@univ-rouen.fr
[b] UMR 6634
[c] UMR 6508

3.8 mm outer diameter, 1.2 mm inner diameter and 140 μm thickness were cut from polycrystalline Fe_3O_4 samples. They were irradiated at room temperature at the GANIL accelerator (Caen, France) by a 5.96 GeV lead ion beam. The projected range ($R_p = 200$ μm) is much higher than the total sample thickness indicating no implantation inside the sample. The maximum electronic stopping power $(dE/dx)_e$ value is about 35 keV/nm. The Pb ion fluences ranged from 4×10^{11} to 3.3×10^{12} ion cm^{-2}.

For the magnetization measurements, a PAR vibrating-sample magnetometer was used with applied fields up to 0.5 T. The sample were mounted with the applied magnetic field parallel to the core surface in order to minimize demagnetizing effects. The measurements of the magnetic hysteresis loops were realized using an hysteresimeter in a low magnetic excitation ($0 < H_a < 100$ A/m) at 2 kHz and a lock amplifier detector. In such a weak applied magnetic field, the observed magnetization is not the saturation magnetization.

3 Experimental results

Saturation magnetization of magnetite exhibits two different domains of variation depending on the ion fluence range. At low fluences, the magnetization first decreases but at high fluence, it reincreases and tends to recover its initial saturation value [9].

The measurements of the magnetic hysteresis cycle were realized on pristine and Pb irradiated samples of magnetite. We recorded the magnetic hysteresis cycles of magnetite samples (Fig. 1) for three irradiation conditions: a pristine sample (a), and two Pb irradiated samples at low (b: 0.8×10^{12} Pb cm^{-2}) fluence and at high (c: 3.3×10^{12} Pb cm^{-2}) fluence.

- The pristine material exhibits a usual hysteresis cycle.
- For the low fluence irradiated sample of magnetite, two remarkable observations can be made: (i) No demagnetization could be observed which would be due to a destruction of the toroidal magnetic configuration. As we know from Mössbauer results, the Pb irradiation of magnetite induces a magnetic anisotropy which results in a rotation of the magnetization perpendicularly to the tracks *i.e.* in the torus plane. (ii) Moreover, the coercive field is 1.7 times higher than the pristine material value. This observation is linked to a pinning of magnetic domain boundaries by columnar defects and to the associated stress observed by electron microscopy.
- For the high fluence, the coercive field and hysteresis cycle have recovered nearly to the same values as for the pristine sample. Such a striking result is in agreement with magnetic (recovering of the magnetization) and crystallographic (drastic decrease of strain effects) results. Thus, upon annealing by track overlap, the effect of columnar defects decreases strongly and the pinning of magnetic domain boundaries vanish.

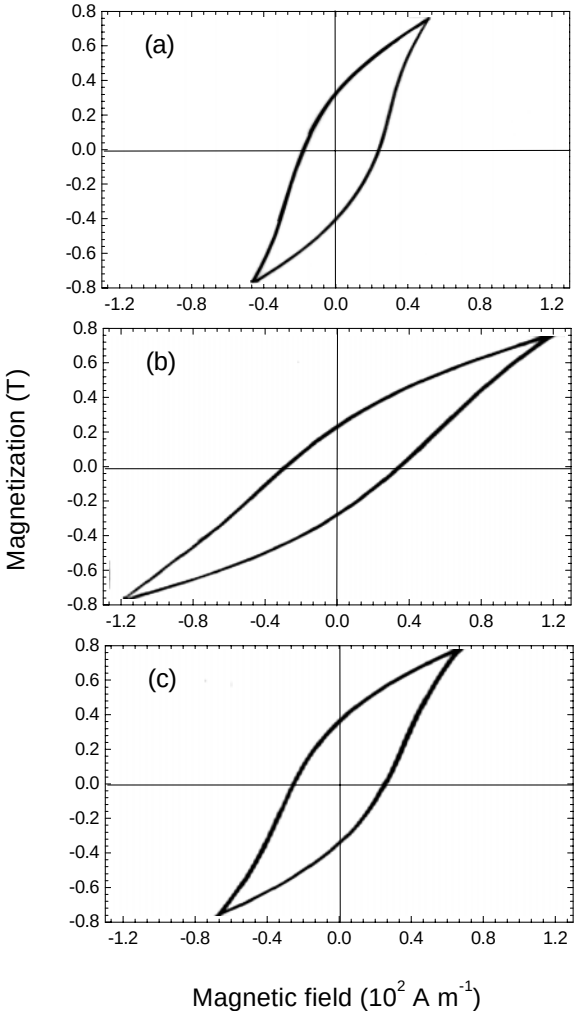

Fig. 1. Magnetic hysteresis loops of magnetite samples irradiated with 6.56 GeV Pb ions: (a) non-irradiated; (b) 0.8×10^{12} Pb cm^{-2}; (c): 3.3×10^{12} Pb cm^{-2}.

4 Damage model

The reorientation of the hyperfine field in irradiated samples, perpendicular or parallel to the tracks, is assumed to result from a magnetoelastic effect according to the sign of the magnetostriction coefficient (λ_s) [9]. In the case of the yttrium iron garnet $Y_3Fe_5O_{12}$ (YIG), this coefficient is negative, but it is positive for the magnetite. The model of damage needs to account for all the experimental observations:

The latent tracks are not amorphous, but remain crystallized with an approximately pristine state, even for high fluences. The saturation magnetization decreases down to a 20% reduction at 1×10^{12} Pb cm^{-2} and then increases for the highest fluence (3.3×10^{12} Pb cm^{-2}), the latter magnetization still exhibiting a small reduction (-5%) with respect to the initial saturation magnetization.

For weak fluences, the latent tracks are surrounded by a stressed cylindrical region (radius R_3) due to the expansion of the matter in latent tracks. In this latter zone,

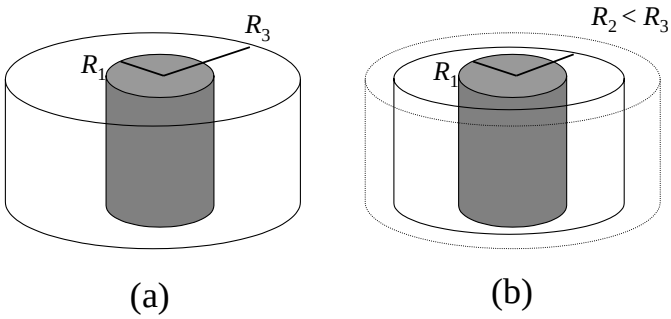

Fig. 2. Scheme of the damage created by a single ion. (a) low fluences; (b) high fluences R_1 = radius of latent track, R_3 = radius of stressed zone at low fluences, R_2 = radius of stressed zone at high fluences.

the magnetization will be oriented following a perpendicular direction to the incident ion path, in agreement with the sign of the magnetostriction coefficient λ_s of the magnetite. Consequently, the magnetization tends to orient radially around tracks (perpendicularly to the axis track). Thereby, areas under stresses have a null resulting magnetization and consequently the total saturation magnetization of the material is decreased.

At higher fluences, *i.e.*, when tracks start to overlap, a new ion track can relax stresses around pre-existing tracks. This phenomenon of stress relaxation by overlapping suppresses the locally blocked perpendicular saturation magnetization, which rotates and tends to orient along the axis of easy magnetization. This hypothesis can explain the reincrease of the saturation magnetization observed at high fluence. Then, the track overlapping participates in the restoration of the magnetic structure of the magnetite.

According to these results, a single-track damage model is proposed to reproduce the fluence dependence of the magnetization in Fe_3O_4. It also allowed to estimate the volumes of the different zones in $Y_3Fe_5O_{12}$.

4.1 Hypotheses of damage model

The single-track model is built using typical laws of damage kinetics [6,10–12]. At low fluences, an incident ion creates in its wake a cylindrical latent track of material of radius R_1 corresponding to a section $S_1 = \pi R_1^2$, which remains crystallized, but contains defects. Outside this cylinder, electronic excitations are not large enough to create defects, but the expansion of matter in the core track induces stresses in a peripheral zone of radius R_3 (section S_3) with $R_3 > R_1$ (Fig. 2). At high fluences, the probability for track overlapping becomes non negligible. We assume that overlapping of the stressed zone of radius R_3 by a new ion track partially relaxes ion-induced stress in this region. Such an assumption is in agreement with the HRTEM observations. We modelize the reduction of the stressed areas at high fluence, by an average reduction of the radius R_3 which takes a new value equal to R_2. We emphasize that in this model the structure of the core-track of radius R_1 is not modified by overlapping effects. The radius values of the damaged and stressed cylinders (R_1 and R_3, respectively), which have a real physical meaning, should be constant in the whole fluence regime and should depend only on the amount of energy deposited by electronic excitations, *i.e.*, on the nature and the energy of the projectile. R_2 takes into account the effective stress volume per ion and should be fluence dependent, starting from R_3 at low fluence to tend toward 0 at high fluences. For the sake of simplicity, we will assume R_2 to be constant with fluence.

4.2 Calculation of the saturation magnetization

Let us define:

- F_1 the damaged fraction of the sample created in the cylinder of radius R_1;
- F_2 the zone fraction that is under stress;
- F_0 the fraction remaining in the initial state (it includes the relaxed fraction).

$$F_0 + F_1 + F_2 = 1. \tag{1}$$

Let M_i be the saturation magnetization of the F_i fraction. The equation that connects the saturation magnetization M_s and the F_i fractions as function of the fluence ϕ can be written as $M_s(\phi) = M_1F_1 + M_0F_0 + M_2F_2$. M_2 is assumed to be zero according to the hypothesis of the model, so:

$$M_s(\phi) = M_0 - (M_0 - M_1)F_1 - M_0F_2. \tag{2}$$

The fluence evolution of the different F_i fractions is given by:

$$\frac{dF_1}{d\phi} = S_1(F_0 + F_2) = S_1(1 - F_1) \tag{3}$$

$$\frac{dF_2}{d\phi} = (S_3 - S_1)F_0 - (S_3 - S_2)F_2 - S_1F_2, \tag{4}$$

where

- S_1F_0 and S_1F_2 correspond respectively to the creation of a track of radius R_1 in the pristine material and in the zone under stresses;
- $(S_3 - S_1)F_0$ corresponds to the creation of a stressed zone in the pristine material;
- $(S_3 - S_2)F_2$ corresponds to the annealed stressed zones during the overlapping of tracks;
- S_1F_2 corresponds to the creation of a track of radius R_1 in the zone under stress.

The solution of equation (3) takes the form of the well known Poisson's law

$$F_1(\phi) = 1 - \exp(-S_1\phi). \tag{5}$$

Using (1), equation (4) becomes:

$$\frac{dF_2}{d\phi} = (S_3 - S_1) - (2S_3 - S_2)F_2 - (S_3 - S_1)F_1. \tag{6}$$

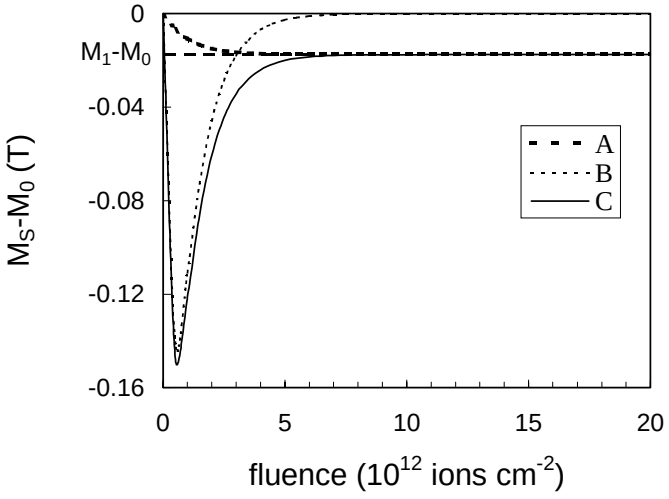

Fig. 3. Graphic representation of the equation (8) that connects the saturation magnetization M_s with the fluence ϕ: curves A and B give respectively the contribution of defects in the track $M_A(\phi)$ and stressed zone around the track $M_B(\phi)$ and the curve C gives the variation of the total magnetization $(M_s(\phi) - M_0)$. $M_1 = M_s(\phi \to \infty)$.

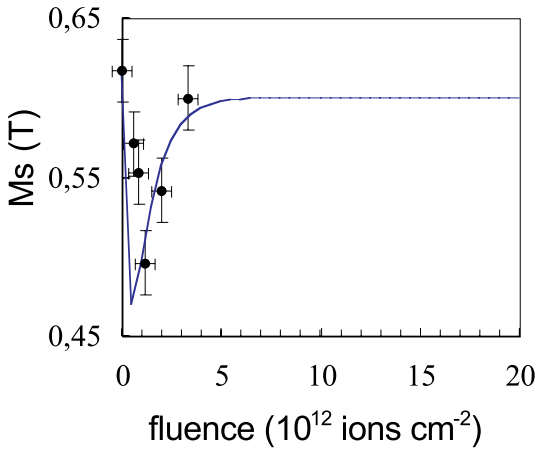

Fig. 4. Experimental and calculated (see text) saturation magnetization for Fe_3O_4 samples as a function of the ion fluence. The samples were irradiated at room temperature with 6.56 GeV Pb ions.

Introducing $S_0 = (2S_3 - S_2)$, the solution of equations (6) can be written as:

$$F_2(\phi) = \frac{(S_3 - S_1)}{(S_0 - S_1)} \left[\exp(-S_1\phi) - \exp(-S_0\phi)\right]. \qquad (7)$$

Substituting these values in the magnetization equation (2) gives:

$$M_s(\phi) = +M_0 + M_A(\phi) + M_B(\phi) \qquad (8)$$

where

$$M_A(\phi) = -(M_0 - M_1)\left[1 - \exp(-S_1\phi)\right]$$

$$M_B(\phi) = -M_0 \frac{(S_3 - S_1)}{(S_0 - S_1)} \left[\exp(-S_1\phi) - \exp(-S_0\phi)\right].$$

This equation (8) decomposes into three terms. The first term M_0 is the saturation magnetization of the pristine material. The terms $M_A(\phi)$ and $M_B(\phi)$ correspond respectively to the defects in the core of tracks and to the stressed shell around the crystallized core which contains defects. Figure 3 displays the variation *versus* the ion fluence of M_A (curve A), M_B (curve B) and $(M_s - M_0)$ (curve C), assuming S_2 constant with fluence. With increasing fluence, M_A decreases (due to accumulation of defects) and tends to a saturation value equal to $-(M_0 - M_1)$. In the case of M_B, there is a first decrease (due to the formation of stressed zone) at low fluence towards a minimum value. The increase of M_B at high fluence is explained by the overlapping of the tracks and then relaxation of the ion-induced stress. Since the variation of $M_s - M_0$ depends on that of M_A and M_B, there is a first decrease of M_s at low fluence, followed by an increase to a saturation value equal to M_1.

Data plotted in Figure 4 are averages of experimental values obtained for two Fe_3O_4 samples irradiated under the same conditions [9]. A least-square fit of the experimental data using equation (8) yields to $S_1 \approx 95 \pm 17$ nm^2 ($R_1 \approx 5.5 \pm 0.5$ nm), $S_2 \approx 95 \pm 17$ nm^2 ($R_2 \approx 5.5 \pm 0.5$ nm) and $S_3 \approx 227 \pm 27$ nm^2 ($R_3 \approx 8.5 \pm 0.5$ nm). Taking into account the experimental errors, the variation of the saturation magnetization *versus* the fluence is suitably reproduced by the model, in spite of its relative simplicity. It is worth noting here that the radius of the central zone calculated with this model ($\approx$5.5 nm) is about four times larger than the one estimated by HRTEM observations. Such a result could be explained by the fact that magnetic transformations are induced at a slightly larger scale than the structural ones.

4.3 Application of the model to the yttrium iron garnet

A similar damage model, based on two crystallized shells surrounding an amorphous core, was used to estimate in swift-heavy-ion irradiated $Y_3Fe_5O_{12}$ the volumes of the three components evidenced by Mössbauer spectrometry [7]. The simulation of the fluence evolution of F_0, F_1 and F_2 volume fractions for irradiated YIG samples is in very good agreement with the experimental values, assuming $R_1 \approx 5 \pm 0.5$ nm, $R_2 \approx 14 \pm 0.5$ nm and $R_3 \approx 20 \pm 0.5$ nm. Then, in the case of YIG, the radius of the magnetic-oriented cylinder is about three times larger than that of Fe_3O_4. This result shows clearly the high sensitivity of the magnetic properties of yttrium iron garnets to heavy-ion irradiation.

The behavior of the magnetite during the irradiation is different from that of the garnet. Indeed, while the cores of tracks are amorphous in $Y_3Fe_5O_{12}$, they remain crystalline in Fe_3O_4, which appears to be very resistant to ion irradiation. Furthermore, the change in reorientation of the magnetic hyperfine field, evidenced by Mössbauer spectrometry for the yttrium garnet and the magnetite, can be linked to the sign of the magnetostriction constant λ_s, accounting for the material distortion along saturation magnetization direction. The coefficient λ_s may be negative, as in the garnet YIG, or positive as in the magnetite Fe_3O_4. This phenomenon is reversible since, upon application of a stress σ, the magnetization may be modified. Inside a magnetic material, the magnetization distribution will depend on the magnetostriction, *i.e.*, on the relationship between magnetic and elastic phenomena (also called magneto-elastic effects).

5 Conclusion

The magnetic properties of the magnetite Fe_3O_4 irradiated by high-energy Pb ions have been investigated by magnetization measurements. In the low fluence regime, an increase of the coercivity due a pinning of magnetic domain boundaries by columnar defects is evidenced. The induced damage and resulting stress strongly affect the magnitude and the direction of the magnetization *via* magnetostrictive effects. For high fluences, the magnetic properties (coercivity and saturation magnetization) of the pristine material are nearly restored, indicating vanishing of domain pinning due to a drastic decrease of stress. The changes of the magnetic properties of ion irradiated magnetite are well described by a phenomenological damage model, based on two strained shells surrounding a core containing various types of defects. This model is also well suited to explain the fluence behavior of the structural and magnetic properties of ion irradiated yttrium iron garnet.

References

1. G. Fuchs, D. Groult, M. Hervieu, N. Nguyen, F. Studer, M. Toulemonde, B. Raveau, *Proceeding of the 3rd European Conference on Solid State Chemitry, Regensburg (1986).*
2. G. Fuchs, E. Balanzat, F. Studer, E. Balanzat, D. Groult, M. Toulemonde, J.C. Jousset, Europhys. Lett. **3**, 321 (1987).
3. F. Studer, D. Groult, N. Nguyen, M. Toulemonde, Nucl. Instrum. Methods Phys. Res. B **19/20**, 856 (1987).
4. F. Studer, M. Hervieu, J.-M. Constantini, M. Toulemonde, Nucl. Instrum. Methods Phys. Res. B **122**, 449 (1997).
5. C. Houpert, F. Studer, D. Groult, M. Toulemonde, Nucl. Instr. Meth. B **39**, 720 (1989).
6. F. Studer, C. Houppert, H. Pascard, R. Spohr, J. Vetter, J.Y. Fan, M. Toulemonde, Radiat. Eff. Defects Sol. **116**, 59 (1991).
7. A. Fnidiki, J. Juraszek, J. Teillet, F. Studer, Appl. Phys. Lett. **75**, 1296 (1999).
8. S. Meillon, F. Studer, M. Hervieu, H. Pascard, Nucl. Instrum. Methods Phys. Res. B **107**, 363 (1996).
9. S. Meillon, Thesis report, Université de Paris XI, Orsay, France (1996).
10. H. Dammak, D. Lesueur, A. Dunlop, P. Legrand, J. Morillo, Radiat. Eff. Defects Sol. **126**, 111 (1993).
11. H. Dammak, D. Lesueur, A. Dunlop, Nucl. Instrum. Methods Phys. Res. B **107**, 204 (1996).
12. A. Dunlop, D. Lesueur, J. Morillo, J. Dural, R. Spohr, J. Vetter, Nucl. Instrum. Methods Phys. Res. B **48**, 419 (1990).
13. A. Audouard, E. Balanzat, J.C. Jousset, A. Chamberod, G. Fuchs, D. Lesueur, L. Thomé, Phil. Mag. B **63**, 727 (1991).